Journal of Materials Chemistry A

PAPER

View Article Online
View Journal | View Issue

Cite this: J. Mater. Chem. A, 2016, 4, 3398

A self-assembled intercalated metal–organic framework electrode with outstanding area capacity for high volumetric energy asymmetric capacitors†

Nobuhiro Ogihara,* Yuka Ozawa and Osamu Hiruta

Received 24th November 2015
Accepted 26th January 2016

DOI: 10.1039/c5ta09559j

www.rsc.org/MaterialsA

The enhancement of the energy of electrochemical capacitors while maintaining high power, long-term cycle stability and safety is challenging. Although there are several types of capacitors that realize high energy density, a system that achieves high energy with safety is still desired. Here we introduce a novel asymmetric capacitor with a negative electrode consisting of an intercalated metal–organic framework (iMOF) composed of 2,6-naphthalene dicarboxylate dilithium, which exhibits a flat plateau near 0.8 V *vs.* Li/Li^+, suitable for high voltage as well as safety. Furthermore, for high volumetric energy density, we propose an extremely thick iMOF electrode prepared by self-assembly of the active material and conductive nanocarbon with an amphiphilic polymer, which possess efficient electron and Li^+ transport pathways, and therefore exhibited an outstanding area capacity of over 2.5 mA h cm^{-2}. Asymmetric capacitors with iMOF negative and activated carbon positive electrodes exhibited a high volumetric energy of 60 W h L^{-1} with favorable power and cycle stability.

Introduction

In energy storage technology for large-scale applications, electrochemical capacitors known as supercapacitors with sufficiently high power capability, which corresponds to a rapid charge–discharge response, play an important role in recovering much of the available energy that is otherwise released as heat.[1,2] Electric double-layer capacitors (EDLCs) with identical electrodes composed of activated carbon (AC) with high specific surface area have such high power capability because their non-faradaic reactions associated with ion adsorption and desorption on the electrode surface exhibit excellent responses. However, EDLCs exhibit lower voltage (2.5 V) and lower energy density (*ca.* 10 W h L^{-1}) than lithium (Li)-ion batteries. Pseudocapacitors containing electrochemical capacitors with high energy density have been proposed,[3] such as manganese oxide (MnO_2), ruthenium oxide (RuO_2),[4,5] nickel hydroxide ($Ni(OH)_2$),[6] two-dimensional transition metal carbides and nitrides (MXenes) in aqueous[7–11] and non-aqueous[12–14] electrolyte systems, molybdenum disulphide (MoS_2) nanosheets in aqueous[15] and non-aqueous[16] electrolyte systems, and metal–organic frameworks (MOFs).[17] However, these systems are currently limited by cell voltages of less than 1.2 V because of the aqueous electrolyte, and the need for thick electrodes increases their mass loading weight,[8,16] so further research is needed.

Asymmetric capacitors consisting of a faradaic intercalation electrode and a non-faradaic electrode in non-aqueous electrolytes have been proposed as an alternative to pseudocapacitors and EDLCs.[18–20] Graphite,[21] $Li_4Ti_5O_{12}$,[22–24] TiO_2–B[25] and *T*-Nb_2O_5 (ref. 20) have been used as intercalation negative electrodes for asymmetric capacitors. An asymmetric capacitor with a graphite electrode exhibited higher voltage close to 4 V and higher energy density (*ca.* 60 W h L^{-1}) than EDLCs.[21] However, graphite operating at 0.05 V (*vs.* Li/Li^+) (Fig. 1) has a safety risk because Li-dendrite deposition can result in an internal short circuit during Li intercalation at a high charging rate[18,26] and/or under low temperature conditions.[27] As a result, the capacity used is limited to less than 20%.[28] Meanwhile, $Li_4Ti_5O_{12}$ operating at 1.55 V has an issue arising from the lower voltage design (1.4–2.8 V) and lower energy density (*ca.* 40 W h L^{-1}) of the cell than graphite.[22,23] Therefore, a negative electrode operating at an intermediate potential between those of graphite and $Li_4Ti_5O_{12}$ would be desirable.

In this work, we report a novel type of asymmetric capacitor with intercalated MOF (iMOF) negative and AC positive electrodes (Fig. 1) to achieve high energy density and suppress the risk of Li-dendrite formation simultaneously, and a proposal of a high-mass loading weight electrode preparation process for the iMOF. Recently, we synthesized an iMOF of 2,6-naphthalene dicarboxylate dilithium crystal (2,6-Naph$(COOLi)_2$) under mild

Toyota Central R&D Laboratories, Inc., Nagakute, Aichi 480-1192, Japan. E-mail: ogihara@mosk.tytlabs.co.jp

† Electronic supplementary information (ESI) available. See DOI: 10.1039/c5ta09559j

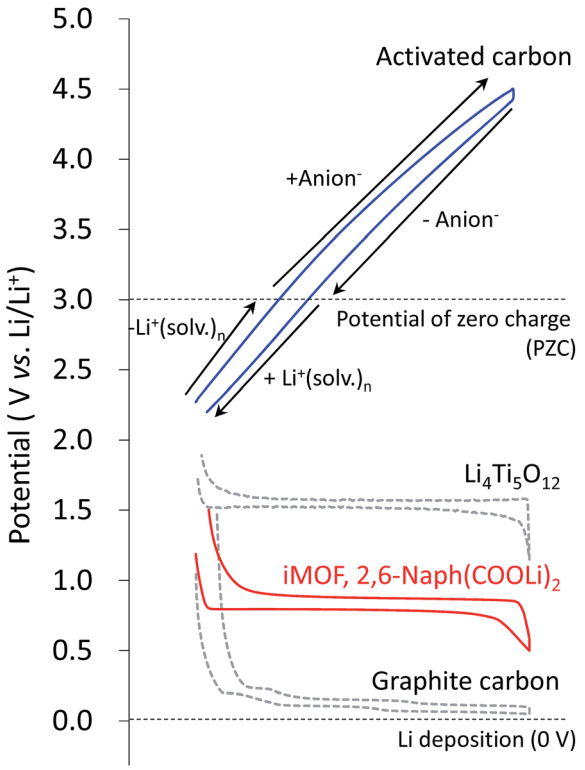

Fig. 1 Comparison of the charge–discharge curves of an iMOF electrode composed of 2,6-Naph(COOLi)$_2$ with those of other possible positive and negative electrodes used in asymmetric capacitors (capacities on the *x*-axis have been normalized).

conditions (see the Sample synthesis in Methods).[29–31] Unlike other reported pseudocapacitive MOF electrode materials, 2,6-Naph(COOLi)$_2$ is nonporous in nature[32] and shows a lithium intercalation reaction with two electron transfer of π-conjugated dicarboxylate operating at 0.8 V, which is between the potentials of graphite and $Li_4Ti_5O_{12}$ (Fig. 1). As shown in Fig. 2, the organic–inorganic layered framework of 2,6-Naph(COOLi)$_2$ was composed of π-stacked naphthalene groups and a tetrahedral LiO_4 network of the carboxylate salt, respectively, providing chemical and electrochemical stability. 2,6-Naph(COOLi)$_2$ has a high density of *ca.* 1.6 g cm^{-3}, reversible specific capacity of 220 mA h g^{-1} and remarkably small volume change (0.33%) during Li intercalation, which is one order of magnitude lower than that of other intercalation electrode materials. By our detailed structural analysis of the lithium intercalated state,[29] the proposed material possesses the tetrahedral LiO_3C network and Li-doped naphthalene packing, which are primarily responsible for Li transport and electronic conduction pathways. Thereby the framework of 2,6-Naph(COOLi)$_2$ (Fig. 2) provides good cycle stability and 2D pathways for both electron and Li^+ transport, allowing a facile redox response.

To design asymmetric capacitors with high energy density, the area capacity ratio of positive and negative electrodes should be optimized at a high loading weight of the active material according to eqn (1).

$$\mathrm{Cap.}_{\mathrm{negative}} m_{\mathrm{negative}} / \mathrm{Cap.}_{\mathrm{positive}} m_{\mathrm{positive}} \quad (1)$$

where Cap. and *m* are the specific capacity (mA h g^{-1}) and mass-loading weight (mg cm^{-2}), respectively. This requires preparation of electrochemically active iMOF electrodes with high loading weight, which leads to high area capacity (mA h cm^{-2}). However, pristine organic electrode materials are mainly electrical insulators, so a large content of conductive carbon (over 50%) is generally required to increase electrode conductivity when using a conventional polyvinylidene fluoride (PVDF) binder, which has hydrophobic properties.[33,34] Therefore, the active material content and loading weight of electrodes are restricted, because it is difficult to disperse slurries of the active material and the conductive carbon agent as electrode coatings. As a result, the area capacities of the reported organic electrodes are limited and do not reach high values (less than 1 mA h cm^{-2}, see Fig. 5). Most of the research has been devoted to the synthesis of new organic compound-based active materials. In

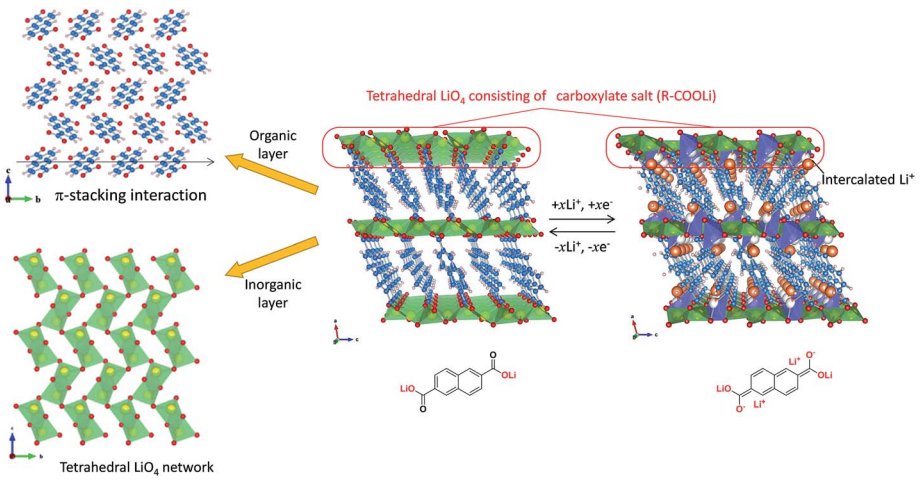

Fig. 2 Structure of the before and after lithium-intercalated 2,6-Naph(COOLi)$_2$ taken from their XRD patterns.[29] Intercalated Li (orange), Li (yellow), O (red), C (blue), and H (white).

contrast, little consideration has been given to the studies on the electrode design to take full advantage of the electrochemical performances of the organic electrode materials, especially for thick electrodes at a high loading weight of active material. Importantly, the experimental energy and power capabilities measured for very thin and/or large amounts of conducting carbon electrodes make only small contributions to actual cell performance.[35,36] Herein, we will report on a high loading weight iMOF electrode through self-assembly using amphiphilic polymers with oxygen-containing functional groups like carboxymethylcellulose (CMC) or polyacrylic acid (PAA) containing both hydrophilic and hydrophobic units that are able to self-assemble in aqueous solutions by non-covalent interactions,[37] which have often been used to synthesize drug delivery agents[38,39] and fluorescent materials.[40]

Experimental

Sample synthesis

The synthesis of 2,6-naphthalene dicarboxylate dilithium (2,6-Naph(COOLi)$_2$) was reported previously.[29] 2,6-Naph(COOLi)$_2$ was synthesized from lithium hydroxide monohydrate (4.85 g, 115.6 mmol) and 2,6-naphthalenedicarboxylic acid (10.0 g, 46.3 mmol) heated under reflux in 300 mL methanol. The solution was initially clear, and then a white precipitate formed over the course of 30 min. The suspension was stirred under reflux conditions for 12 h. The mixture was evaporated, and then the resulting solid was washed with methanol, and dried under ambient conditions. The product was obtained as needle-shaped white crystals (96.8% yield based on 2,6-Naph(COOLi)$_2$).

Electrode and electrolyte preparations

Amphiphilic polymer-based 2,6-Naph(COOLi)$_2$ electrodes were prepared by coating a dispersion of 77–82 wt% 2,6-Naph(COOLi)$_2$, 13–14 wt% carbon black as a conductive agent, 2–6 wt% carboxymethylcellulose (CMC) or polyacrylic acid (PAA) as an amphiphilic polymer, and 2–4 wt% styrene butadiene rubber (SBR) as a binder in water onto Cu foil. Electrode loading weights of *ca.* 2, 4, 6, 8, 12 and 14 mg cm^{-2} were used. Conventional PVDF-based 2,6-Naph(COOLi)$_2$ electrodes were prepared by coating a dispersion of 79.6 wt% 2,6-Naph(COOLi)$_2$, 13.0 wt% carbon black or carbon black with vapor-grown carbon fibers as a conductive agent, and 7.4 wt% PVDF binder in *N*-methyl-2-pyrrolidone onto Cu foil for comparison. The electrode loading weight was *ca.* 2 mg cm^{-2}. Activated carbon (AC)-based electrodes were also prepared by coating a dispersion of 83 wt% AC (Kurare YP-20), 10.7 wt% carbon black, 4 wt% CMC, and 2.3 wt% SBR in water onto Al foil. The electrode loading weight was *ca.* 2 or 3 mg cm^{-2}. All electrodes were dried at 120 °C under vacuum for at least 10 h before constructing electrochemical cells. The electrolytes in this study were 1 M $LiPF_6$ dissolved in a solution of ethylene carbonate (EC), dimethyl carbonate (DMC), and ethyl methyl carbonate (EMC) (volume ratio of 30 : 40 : 30, respectively) and 1 M triethylmethylammonium tetrafluoroborate (NEt_3MeBF_4) dissolved in a solution of propylene carbonate. A microporous polypropylene film was used as the separator.

Morphology characterization

The surface morphology of 2,6-Naph(COOLi)$_2$ crystals and 2,6-Naph(COOLi)$_2$ electrodes was examined by scanning electron microscopy (SEM, S-5500, Hitachi, Japan). Samples for cross-sectional SEM analysis were prepared by an *in situ* focused ion beam (FIB) technique. Images were recorded using a SEM (NB5000 nanoDUE'T FIB-SEM, Hitachi) operating at 2 kW. Cross-sectional images and elemental mapping of the 2,6-Naph(COOLi)$_2$ electrodes were obtained by electron probe microanalysis (EPMA) (JXA-8500F JEOL, Japan) using an acceleration voltage of 7 kV and beam current of 50 nA. Prior to EPMA, the samples were embedded in epoxy resin (EpoFix, Struers) and cross-sectional samples were prepared using a FIB.

Electrochemical characterization

The electrochemical properties of Li/2,6-Naph(COOLi)$_2$ and 2,6-Naph(COOLi)$_2$/AC cells were examined using coin- and laminate-type cells, respectively, assembled with a separator filled with an $LiPF_6$-based electrolyte in an argon-filled glove box. In galvanostatic charge–discharge measurements to determine the specific capacity and electrochemical reversibility of the 2,6-Naph(COOLi)$_2$ electrodes at 25 °C, coin-type cells were cycled between 0.5 and 2.0 V *vs.* Li/Li$^+$ at a rate corresponding to fully charging the theoretical capacity of 2,6-Naph(COOLi)$_2$ per 10 h at *ca.* 2, 4, 6 and 8 mg cm^{-2} and 20 h at *ca.* 12 and 14 mg cm^{-2}. For laminate-type cells, an AC electrode was used as the positive electrode, and a Li pre-doped 2,6-Naph(COOLi)$_2$ electrode was used as the negative electrode. The electrolyte was the same as that in the coin-type cells. For comparison, EDLCs with identical AC electrodes were assembled with a separator filled with a NEt_3MeBF_4-based electrolyte. Galvanostatic charge–discharge measurements of the 2,6-Naph(COOLi)$_2$/AC asymmetric capacitors and EDLCs were conducted at 25 °C between 1.5 and 3.8 V, and 0.0 and 2.5 V, respectively, at various current densities between 1 and 100 mA cm^{-2} to determine energy and power densities. Prior to galvanostatic charge–discharge measurements of the asymmetric capacitors, cells containing 2,6-Naph(COOLi)$_2$ and Li metal electrodes with a separator were prepared. These cells were cycled between 0.5 and 2.0 V under the same rate conditions as the coin-type cells and the state of charge (SOC) of the 2,6-Naph(COOLi)$_2$ electrodes was set at 50%. Asymmetric capacitors were then prepared using the 2,6-Naph(COOLi)$_2$ electrodes taken from these cells and the AC electrodes.

Electrochemical impedance spectroscopy using a symmetric cell[35,41] was performed to determine the ionic resistance (R_{ion}) of the porous 2,6-Naph(COOLi)$_2$ electrodes. To do this, identical 2,6-Naph(COOLi)$_2$ electrodes were assembled with a separator filled with a $LiPF_6$-based electrolyte. Electrochemical impedance measurements (Solatron 1260/1286, England) of symmetric cells were performed at an open-circuit potential. The frequency was varied from 100 kHz to 100 mHz with

a perturbation amplitude of 10 mV (peak to peak). Measurements were performed between −10 and 60 °C.

Results and discussion

Firstly, we prepare extremely thick electrodes having a high electrochemical activity through self-assembly using amphiphilic polymers, iMOF particles and conductive nanocarbon materials. The schematic illustration in Fig. 3a shows the self-assembled electrode preparation procedure. The crystal surface of 2,6-Naph(COOLi)$_2$ shows hydrophilic properties because of carboxylate units (Fig. 2). In contrast, the surface of the conducting nanocarbon shows hydrophobic properties. Therefore, the self-assembly between 2,6-Naph(COOLi)$_2$ and conductive nanocarbon was attempted by hydrophilic and hydrophobic interactions of amphiphilic polymers in aqueous slurry for electrode coating. As shown in Fig. 3b, aqueous slurries of 2,6-Naph(COOLi)$_2$ and conductive nanocarbon with and without the amphiphilic polymer are black and gray, respectively. This indicates that the white 2,6-Naph(COOLi)$_2$ particles are covered by black conductive nanocarbon in the slurry with the amphiphilic polymer, whereas the surface of 2,6-Naph(COOLi)$_2$ is exposed in the slurry without the amphiphilic polymer. This means that the hydrophilic carboxylate groups on the side chains and the hydrophobic main chain of the amphiphilic polymer interact with carboxylate groups on the surface of the 2,6-Naph(COOLi)$_2$ crystal and hydrophobic conductive nanocarbon in solution, respectively. At low carbon contents, cross-sectional images of the electrodes prepared by coating of the self-assembled aqueous slurry confirmed that 2,6-Naph(COOLi)$_2$ particles were covered with conductive nanocarbon and revealed uniform pore structures in the depth direction (Fig. 3c and d). Although pristine 2,6-Naph(COOLi)$_2$ consists of needle-shaped crystals with hundreds of nanosized irregularities resembling intestinal villus (Fig. S1†), the irregularities in the self-assembled electrode are coated with conductive nanocarbon (Fig. S2†). This indicates that an optimal electron transfer interface can form between 2,6-Naph(COOLi)$_2$ and conductive nanocarbon through self-assembly driven by an amphiphilic polymer. Conversely, aggregation of the conductive nanocarbon was observed without covering 2,6-Naph(COOLi)$_2$ particles in the electrode prepared using the conventional polyvinylidene fluoride (PVDF) binder (Fig. S3†).

Next, the electrochemical performance of the self-assembled 2,6-Naph(COOLi)$_2$ electrode was examined in cells using Li metal as the counter electrode. The self-assembled 2,6-Naph(COOLi)$_2$ electrode has advantages of (i) low conductive nanocarbon content, (ii) high mass-loading weight and (iii) reversible electrochemistry. As shown in Fig. S4,† charge–discharge profiles measured for Li/2,6-Naph(COOLi)$_2$ cells confirmed that the 2,6-Naph(COOLi)$_2$ electrode prepared using the amphiphilic polymer CMC possessed higher specific capacity, which corresponds to approximately the theoretical capacity of 2e$^-$ and 2Li$^+$ per molecule, compared to that prepared using PVDF under the same conditions, and favorable

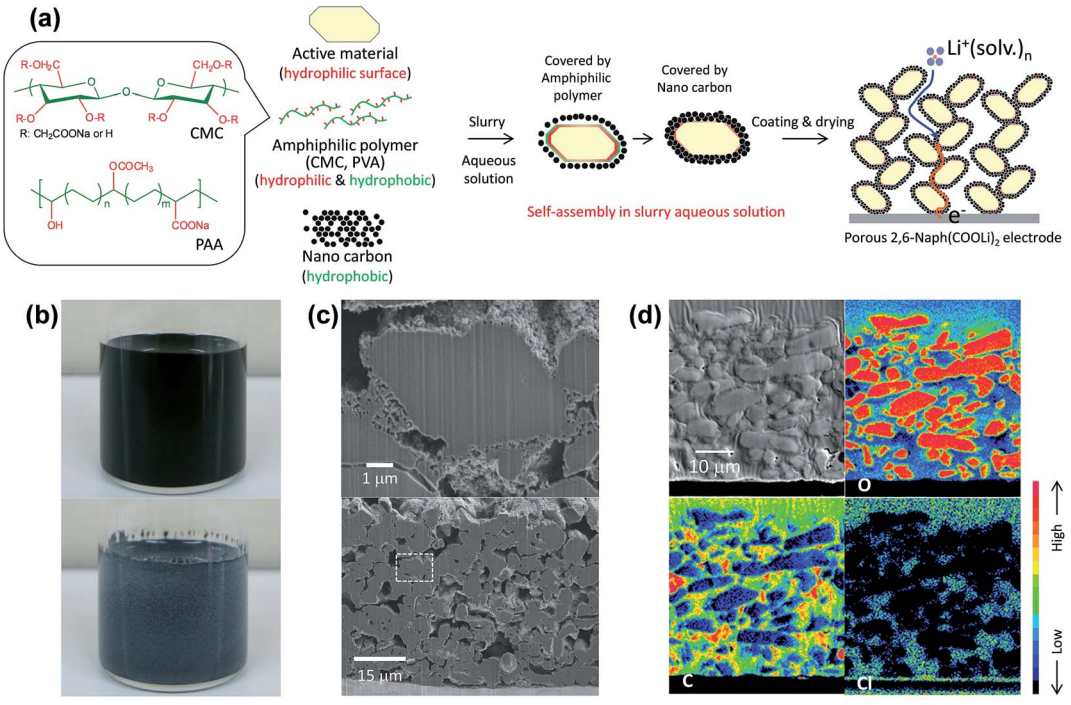

Fig. 3 (a) Schematic illustration of preparation of a porous 2,6-Naph(COOLi)$_2$ electrode from a slurry of the active material and conductive nanocarbon with the amphiphilic polymer. (b) Photographs of slurries of 2,6-Naph(COOLi)$_2$ and conductive nanocarbon with (top) and without (bottom) amphiphilic polymer CMC. (c) Cross-sectional scanning electron micrographs of the porous 2,6-Naph(COOLi)$_2$ electrode. (d) Cross-sectional electron probe microanalysis mapping of oxygen, carbon and chlorine in the prepared electrode, which correspond to 2,6-Naph(COOLi)$_2$ particles, conductive nanocarbon and pore structure filled with resin containing chlorine, respectively.

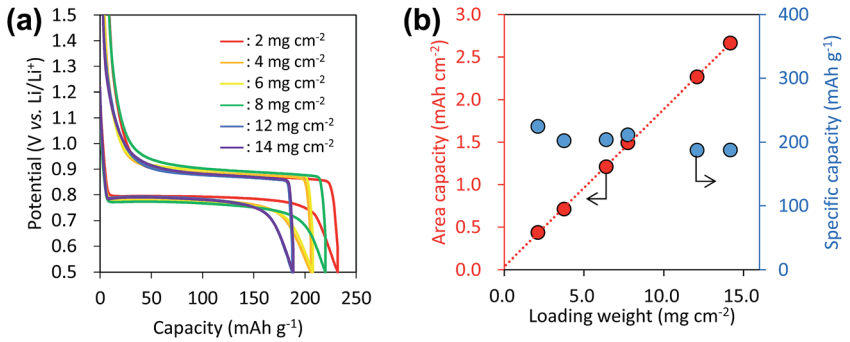

Fig. 4 (a) Comparison of steady-state charge–discharge profiles of Li/2,6-Naph(COOLi)$_2$ cells containing electrodes with loading weights of *ca.* 2, 4, 6, 8, 12 and 14 mg cm^{-2}. (b) Dependence of area capacity and specific capacity of 2,6-Naph(COOLi)$_2$ electrodes on loading weight.

rate capabilities (Fig. S5†). This means that the self-assembled 2,6-Naph(COOLi)$_2$ electrode gives a reversible redox response at a small amount of conductive carbon ratio by uniform coating of conductive carbon onto 2,6-Naph(COOLi)$_2$ particles, as shown in Fig. 3c and d.

Importantly, as shown in Fig. 4a, the self-assembled 2,6-Naph(COOLi)$_2$ electrode maintained high reversible specific capacities and small polarization at a high loading weight of *ca.* 14 mg cm^{-2}. The area capacity increased linearly with loading weight, and reached an outstanding value of 2.66 mA h cm^{-2} (Fig. 4b). This value is five times higher than those reported for organic electrode materials of Li-based (0.5–0.7 mA h cm^{-2})[42–45] and Na-based (0.2–0.5 mA h cm^{-2})[46–49] electrolyte systems (Fig. 5), and comparable to those of high-capacity silicon-based negative electrodes for Li-ion batteries (0.13–5.00 mA h cm^{-2}) (Fig. S6†).

To gain further insight into the ionic resistance in pores (R_{ion}) and the corresponding ionic conductivity of the prepared porous 2,6-Naph(COOLi)$_2$ electrodes, electrochemical impedance spectroscopy using symmetric cells that assemble the identical 2,6-Naph(COOLi)$_2$ electrodes with the separator filled with the electrolyte[35,41] was conducted. This technique can focus on the impedance of a single electrode without affecting the other electrodes. Although the electrodes with high loading weights of *ca.* 12 and 14 mg cm^{-2} exhibited relatively high resistance at high frequencies of over 1 kHz (Fig. S7†), as shown in Fig. 6a, the plots were linear with a 45° slope and vertical from the real axis in the middle- and low-frequency regions, respectively, which is the typical electrical blocking behavior of porous electrodes without a charge–transfer reaction. R_{ion} obtained by fitting (see the ESI and Fig. S8†) increased linearly with loading weight (Fig. 6b). This indicates an ideal ionic resistance related to the mass-loading weight as shown in eqn (S3) in the ESI.† Therefore, the ionic conductivity in electrode pores was constant for all electrode thicknesses (Fig. 6b) and also exhibited identical temperature dependence regardless of loading weight (Fig. S9†). The use of CMC and its analogs as binders has demonstrated improvement of cycle stability due to high adhesion for graphite carbon or silicon negative electrode materials.[50–53] Unlike the previous reports, key finding of this study is that amphiphilic polymers have a high selectivity for both the iMOF and conducting carbon surfaces, whereas hydrophobic PVDF selects only the hydrophobic conducting carbon. Thereby, the conductive carbon is uniformly coated on the iMOF surface in small amounts of conducting carbons with amphiphilic polymers. Therefore, the self-assembled iMOF electrode can lead to practically useful electrochemical performance in a wide range of loading weights.

Finally, an asymmetric capacitor composed of Li-pre-doped 2,6-Naph(COOLi)$_2$ negative and AC positive electrodes was constructed in a laminate-type cell. As shown in Fig. 7a, the asymmetric capacitor exhibited a higher voltage range of 1.5–3.8 V compared with the EDLC. This asymmetric capacitor utilized the high electric double-layer capacitances of both PF_6^- anions and Li^+ cations at the AC positive electrode by the pre-doping treatment with Li. This has been confirmed by the results of the differential capacity dQ/dV plots of the same cells (Fig. S10†). The asymmetric capacitor also showed long-term cycle stability with a retention of 86% after 1000 cycles (Fig. 7b). Previously we have confirmed that there is no change of obvious

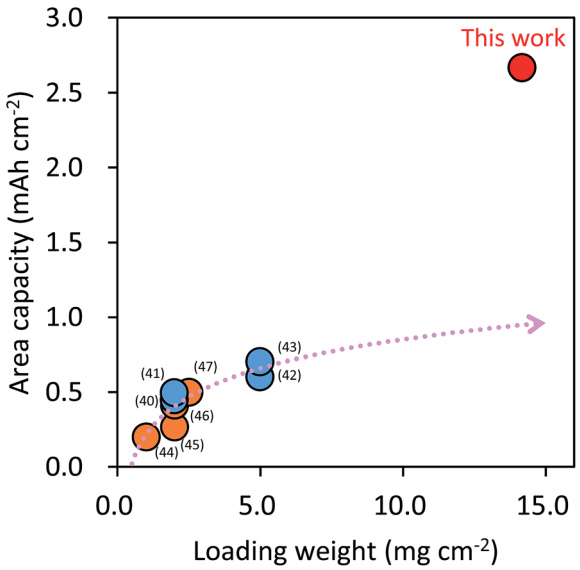

Fig. 5 Comparison of the area capacity of 2,6-Naph(COOLi)$_2$ electrodes with a high loading weight with those of other reported organic redox electrode materials (blue: Li-base,[42–45] and orange: Na-base[46–49]). The arrow is an approximate curve estimated by the least squares method in the reported values.

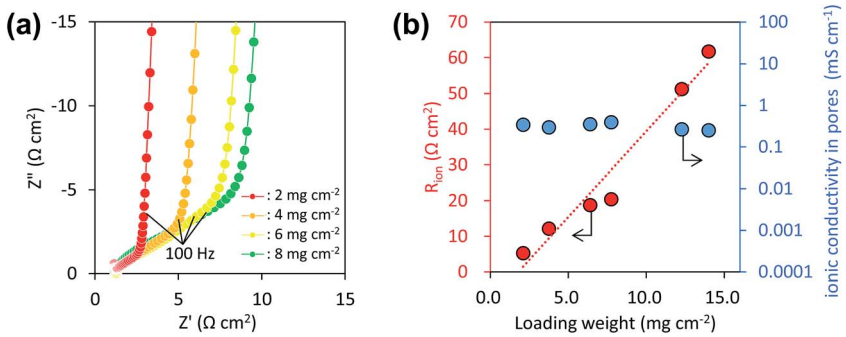

Fig. 6 (a) Nyquist plots for symmetric cells containing two identical 2,6-Naph(COOLi)$_2$ electrodes with loading weights of *ca.* 2, 4, 6 and 8 mg cm^{-2} at 25 °C. (b) Dependence of ionic resistance and conductivity of pores of 2,6-Naph(COOLi)$_2$ electrodes (obtained by fitting with the transmission line model) on loading weight.

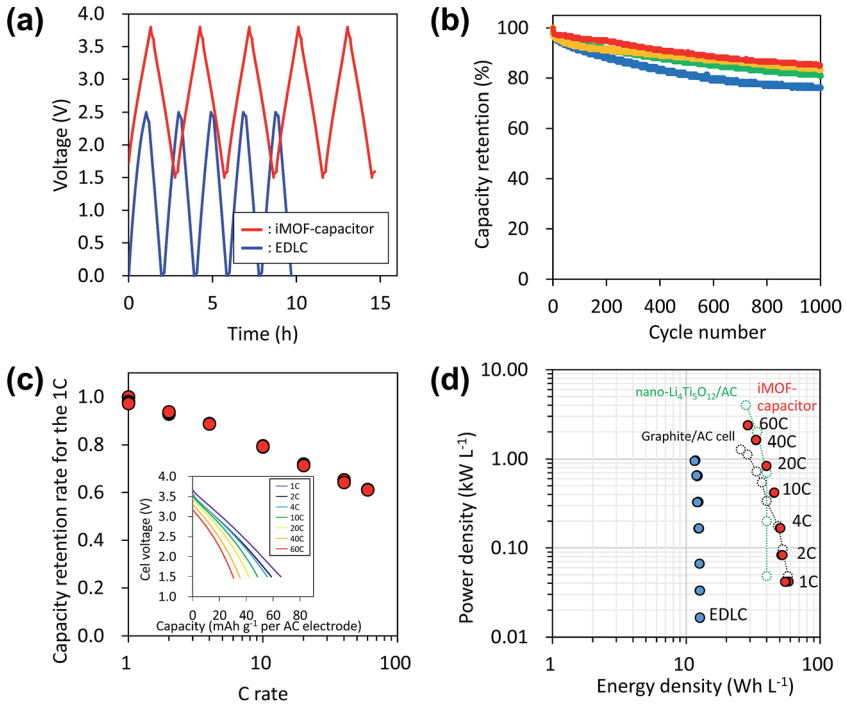

Fig. 7 (a) Galvanostatic charge–discharge curves of the proposed asymmetric capacitor (iMOF-capacitor) and EDLC at the same loading weight for an AC positive electrode and current density. (b) Cycling capacity retention of asymmetric capacitors at a charge–discharge rate of 10C. The capacity ratio of the negative electrode to the positive electrode was 2.7. The ratio of active material to conductive nanocarbon was (blue) 85 : 15, (green) 81 : 19, (yellow) 77 : 23 and (red) 74 : 26. (c) Rate capability of the optimized cell is shown in Fig. S11.† Inset: discharge curves of the same cell at rates from 1 to 60C. (d) Comparison of volumetric energy *versus* power of the asymmetric capacitor, EDLC and other reported asymmetric capacitors, such as graphite/AC[21] and $Li_4Ti_5O_{12}$/AC[22] cells.

size, shape and crystal structure before and after cycling.[29] This result in this study suggests that the favorable cycle performances of the proposed asymmetric capacitor are attributed to a very small volume strain during Li intercalation and the insolubility of the self-assembled 2,6-Naph(COOLi)$_2$ electrode in common organic electrolytes. The energy and power performances of the capacitor were optimized according to eqn (1) for preferable electrode conditions[36] (Fig. S11†). The capacitor can be discharged under high rate conditions (discharge for 1 min at 60C) (Fig. 7c, inset). The retention rate at 60C is *ca.* 60% (Fig. 7c), which is close to that of the pseudocapacitive electrode material orthorhombic *T*-Nb_2O_5, which has high rate capability,[20] and better than that of other Na-based asymmetric capacitors with MXene electrode materials, such as a Ti_2CT_x (negative)/$Na_2Fe(S_4O_4)_3$ (positive) capacitor[54] or a hard carbon/V_2C capacitor.[14] The proposed asymmetric capacitor exhibited high gravimetric and volumetric energy (*ca.* 80 W h kg^{-1} and 60 W h L^{-1}, respectively) and gravimetric and volumetric power (*ca.* 3.2 kW kg^{-1} and 2.3 kW L^{-1}, respectively) (Fig. 7d). Overall, the capacitor exhibits an energy density that is five to six times higher than that of typical EDLCs as well as comparable power density, higher power density than a graphite/AC capacitor

(*ca.* 1.2 kW L^{-1}),[21] and higher energy density than a $Li_4Ti_5O_{12}$/AC capacitor (*ca.* 55 W h kg^{-1}, 40 W h L^{-1}).[22] Although these results reveal excellent full-cell performance compared to reported asymmetric capacitors optimized by Li pre-doping[21] or using nanosized active materials[22] to maximize rate capability, the power capability of the proposed asymmetric capacitors can still be further improved.

Conclusions

In summary, the use of an iMOF, 2,6-Naph$(COOLi)_2$, electrode material was demonstrated as an effective approach for advanced asymmetric capacitors. This work developed an outstanding area capacity on the iMOF electrode through self-assembly using amphiphilic polymers, which allows efficient electron and Li^+ transport not only in the bulk crystal but also in the porous electrodes. Therefore, the proposed asymmetric capacitors with iMOF electrodes possess both high volumetric energy and power with safety. This study is a new approach to organic-based electrodes. Thus, we believe that our finding of self-assembled thick electrodes composed of iMOF not only reveals the feasibility of organic-based electrode materials, but also advances the evolution of supercapacitors.

Acknowledgements

We acknowledge Ms. Y. Matsuoka, Mr J. Seki and Mr Y. Yagi for morphology characterization and Dr T. Sasaki for fruitful discussion.

References

1 J. R. Miller and P. Simon, *Science*, 2008, **321**, 651–652.
2 P. Simon, Y. Gogotsi and B. Dunn, *Science*, 2014, **343**, 1210–1211.
3 V. Augustyn, P. Simon and B. Dunn, *Energy Environ. Sci.*, 2014, **7**, 1597.
4 J. P. Zheng, P. J. Cygan and T. R. Jow, *J. Electrochem. Soc.*, 1995, **142**, 2699–2703.
5 W. Sugimoto, H. Iwata, Y. Yasunaga, Y. Murakami and Y. Takasu, *Angew. Chem., Int. Ed. Engl.*, 2003, **42**, 4092–4096.
6 H. B. Li, M. H. Yu, F. X. Wang, P. Liu, Y. Liang, J. Xiao, C. X. Wang, Y. X. Tong and G. W. Yang, *Nat. Commun.*, 2013, **4**, 1894.
7 M. R. Lukatskaya, O. Mashtalir, C. E. Ren, Y. Dall'Agnese, P. Rozier, P. L. Taberna, M. Naguib, P. Simon, M. W. Barsoum and Y. Gogotsi, *Science*, 2013, **341**, 1502–1505.
8 M. Ghidiu, M. R. Lukatskaya, M. Q. Zhao, Y. Gogotsi and M. W. Barsoum, *Nature*, 2014, **516**, 78–81.
9 Z. Ling, C. E. Ren, M.-Q. Zhao, J. Yang, J. M. Giammarco, J. Qiu, M. W. Barsoum and Y. Gogotsi, *Proc. Natl. Acad. Sci. U. S. A.*, 2014, **111**, 16676–16681.
10 M. Q. Zhao, C. E. Ren, Z. Ling, M. R. Lukatskaya, C. Zhang, K. L. Van Aken, M. W. Barsoum and Y. Gogotsi, *Adv. Mater.*, 2015, **27**, 339–345.
11 M. R. Lukatskaya, S.-M. Bak, X. Yu, X.-Q. Yang, M. W. Barsoum and Y. Gogotsi, *Adv. Energy Mater.*, 2015, **5**, 1500589.
12 M. Naguib, J. Come, B. Dyatkin, V. Presser, P.-L. Taberna, P. Simon, M. W. Barsoum and Y. Gogotsi, *Electrochem. Commun.*, 2012, **16**, 61–64.
13 M. Naguib, J. Halim, J. Lu, K. M. Cook, L. Hultman, Y. Gogotsi and M. W. Barsoum, *J. Am. Chem. Soc.*, 2013, **135**, 15966–15969.
14 Y. Dall'Agnese, P. L. Taberna, Y. Gogotsi and P. Simon, *J. Phys. Chem. Lett.*, 2015, **6**, 2305–2309.
15 H. Tang, J. Wang, H. Yin, H. Zhao, D. Wang and Z. Tang, *Adv. Mater.*, 2015, **27**, 1117–1123.
16 M. Acerce, D. Voiry and M. Chhowalla, *Nat. Nanotechnol.*, 2015, **10**, 313–318.
17 K. M. Choi, H. M. Jeong, J. H. Park, Y.-B. Zhang, J. K. Kang and O. M. Yaghi, *ACS Nano*, 2014, **8**, 7451–7457.
18 I. Plitz, A. DuPasquier, F. Badway, J. Gural, N. Pereira, A. Gmitter and G. G. Amatucci, *Appl. Phys. A*, 2005, **82**, 615–626.
19 A. Yoshino, T. Tsubata, M. Shimoyamada, H. Satake, Y. Okano, S. Mori and S. Yata, *J. Electrochem. Soc.*, 2004, **151**, A2180.
20 V. Augustyn, J. Come, M. A. Lowe, J. W. Kim, P. L. Taberna, S. H. Tolbert, H. D. Abruna, P. Simon and B. Dunn, *Nat. Mater.*, 2013, **12**, 518–522.
21 J. Zhang, Z. Q. Shi and C. Y. Wang, *Electrochim. Acta*, 2014, **125**, 22–28.
22 K. Naoi, S. Ishimoto, J.-I. Miyamoto and W. Naoi, *Energy Environ. Sci.*, 2012, **5**, 9363.
23 K. Naoi, S. Ishimoto, Y. Isobe and S. Aoyagi, *J. Power Sources*, 2010, **195**, 6250–6254.
24 H.-G. Jung, N. Venugopal, B. Scrosati and Y.-K. Sun, *J. Power Sources*, 2013, **221**, 266–271.
25 V. Aravindan, N. Shubha, W. C. Ling and S. Madhavi, *J. Mater. Chem. A*, 2013, **1**, 6145–6151.
26 L. Yang, X. Cheng, Y. Gao, P. Zuo, Y. Ma, C. Du, B. Shen, Y. Cui, T. Guan and G. Yin, *ACS Appl. Mater. Interfaces*, 2014, **6**, 12962–12970.
27 G. Park, N. Gunawardhana, H. Nakamura, Y.-S. Lee and M. Yoshio, *J. Power Sources*, 2012, **199**, 293–299.
28 V. Khomenko, E. Raymundo-Piñero and F. Béguin, *J. Power Sources*, 2008, **177**, 643–651.
29 N. Ogihara, T. Yasuda, Y. Kishida, T. Ohsuna, K. Miyamoto and N. Ohba, *Angew. Chem., Int. Ed. Engl.*, 2014, **53**, 11467–11472.
30 T. Yasuda and N. Ogihara, *Chem. Commun.*, 2014, **50**, 11565–11567.
31 N. Ogihara and Y. Kishida, *Electrochemistry*, 2015, **83**, 861–863.
32 D. Banerjee, S. J. Kim and J. B. Parise, *Cryst. Growth Des.*, 2009, **9**, 2500–2503.
33 Z. Zhang, H. Yoshikawa and K. Awaga, *J. Am. Chem. Soc.*, 2014, **136**, 16112–16115.
34 S. Gottis, A. L. Barres, F. Dolhem and P. Poizot, *ACS Appl. Mater. Interfaces*, 2014, **6**, 10870–10876.
35 N. Ogihara, Y. Itou, T. Sasaki and Y. Takeuchi, *J. Phys. Chem. C*, 2015, **119**, 4612–4619.

36 Y. Gogotsi and P. Simon, *Science*, 2011, **334**, 917–918.
37 C. Wang, Z. Wang and X. Zhang, *Acc. Chem. Res.*, 2012, **45**, 608–618.
38 W.-C. Huang, S.-Y. Chen and D.-M. Liu, *Soft Matter*, 2012, **8**, 10868.
39 W. C. Huang, H. Y. Lai, L. W. Kuo, C. H. Liao, P. H. Chang, T. C. Liu, S. Y. Chen and Y. Y. Chen, *Adv. Mater.*, 2015, **27**, 4186–4193.
40 X. Wang, Y. Guo, D. Li, H. Chen and R. C. Sun, *Chem. Commun.*, 2012, **48**, 5569–5571.
41 N. Ogihara, S. Kawauchi, C. Okuda, Y. Itou, Y. Takeuchi and Y. Ukyo, *J. Electrochem. Soc.*, 2012, **159**, A1034–A1039.
42 S. Wang, L. Wang, K. Zhang, Z. Zhu, Z. Tao and J. Chen, *Nano Lett.*, 2013, **13**, 4404–4409.
43 Z. Song, Y. Qian, X. Liu, T. Zhang, Y. Zhu, H. Yu, M. Otani and H. Zhou, *Energy Environ. Sci.*, 2014, **7**, 4077–4086.
44 W. Walker, S. Grugeon, O. Mentre, S. Laruelle, J.-M. Tarascon and F. Wudl, *J. Am. Chem. Soc.*, 2010, **132**, 6517–6523.
45 W. Walker, S. Grugeon, H. Vezin, S. Laruelle, M. Armand, F. Wudl and J.-M. Tarascon, *J. Mater. Chem.*, 2011, **21**, 1615.
46 A. Choi, Y. K. Kim, T. K. Kim, M. S. Kwon, K. T. Lee and H. R. Moon, *J. Mater. Chem. A*, 2014, **2**, 14986–14993.
47 W. Luo, M. Allen, V. Raju and X. L. Ji, *Adv. Energy Mater.*, 2014, **4**, 1400554.
48 S. Wang, L. Wang, Z. Zhu, Z. Hu, Q. Zhao and J. Chen, *Angew. Chem., Int. Ed. Engl.*, 2014, **53**, 5892–5896.
49 A. Abouimrane, W. Weng, H. Eltayeb, Y. Cui, J. Niklas, O. Poluektov and K. Amine, *Energy Environ. Sci.*, 2012, **5**, 9632–9638.
50 H. Buqa, M. Holzapfel, F. Krumeich, C. Veit and P. Novák, *J. Power Sources*, 2006, **161**, 617–622.
51 J. Li, R. B. Lewis and J. R. Dahn, *Electrochem. Solid-State Lett.*, 2007, **10**, A17–A20.
52 I. Kovalenko, B. Zdyrko, A. Magasinski, B. Hertzberg, Z. Milicev, R. Burtovyy, I. Luzinov and G. Yushin, *Science*, 2011, **334**, 75–79.
53 L. Jabbour, C. Gerbaldi, D. Chaussy, E. Zeno, S. Bodoardo and D. Beneventi, *J. Mater. Chem.*, 2010, **20**, 7344.
54 X. Wang, S. Kajiyama, H. Iinuma, E. Hosono, S. Oro, I. Moriguchi, M. Okubo and A. Yamada, *Nat. Commun.*, 2015, **6**, 6544.